

# Multi-Modal Built-In Self-Test for Symmetric Microsystems\*

Nilmoni Deb and R. D. (Shawn) Blanton  
Center for Silicon System Implementation  
Department of Electrical and Computer Engineering  
Carnegie Mellon University  
Pittsburgh, PA 15213  
email: {ndeb, blanton}@ece.cmu.edu

## Abstract

*A mathematical model analyzing the efficacy of a built-in self-test technique, applicable to any symmetrical MEMS microstructure, is developed. The model predicts that the BIST technique can also be used to characterize a wide range of local manufacturing variations affecting different regions of the device. Model predictions have been validated by simulation. Specifically, it has been shown that by using a suitable modulation scheme, sensitivity to linear etch variation along a particular direction is improved by nearly 30%.*

## 1 Introduction

The increasing need for multi-functional sensor and actuator systems that are capable of real-time interaction with both electrical and non-electrical environments has led to the development of a very broad class of “Microsystems”. Microsystems are heterogeneous [1] since they are based on the interactions of multiple energy domains that can include electrical, mechanical, optical, thermal, chemical and fluidic. Major classes of microsystems include MicroElectroMechanical Systems (MEMS), MicroOptoElectroMechanical Systems (MOEMS), and systems that include thermal and fluidic components. Reliable manufacture of affordable microsystems naturally requires the use of cost-effective test methods that isolate malfunctioning systems from good ones. The multi-domain nature of microsystems makes them inherently complex for both design and test. In addition, the increasing number of devices integrated on chip has added to the challenge of microsystem testing. Finally, the growing use of microsystems in life-critical applications such as air-bags [2], bio-sensors [3] and satellites [4] has accelerated the need for high reliability that cannot be achieved without the use of robust test methods.

Among currently used MEMS process technologies, surface micromachining [5] is widely deployed due to its similarity to thin-film technology used for integrated circuits. Surface micromachining is already proven to be a technology that is

commercially viable since it can support high-volume manufacture of MEMS devices. Example applications of this technology include the digital micromirror display [6] and the accelerometer [7, 8]. Our work in microsystem test has therefore been focussed on surface-micromachined devices. However, the built-in test method analyzed here is also applicable to other process technologies.

The objective of manufacturing test is to identify malfunctioning devices in a batch of fabricated devices. Device malfunction is caused by various failure sources in the manufacturing process that include but are not limited to foreign particles [9], etch variations and stiction [10, 11], each of which can lead to a variety of defects. When defects cause the device performance to go “out-of-spec”, the device is said to have failed. However, test has limitations which can cause good devices to be rejected (yield loss) and bad devices to be accepted (test escape). The cost of test escape can exceed the cost of yield loss since a device that passes traditional, specification-based manufacturing test may fail in the field with catastrophic results [12]. One of the aims of built-in self test (BIST) is the prevention of field failures.

Commercially-manufactured MEMS are usually affected by multiple failure sources. Defects caused by many of these failure sources exhibit very similar misbehaviors and are therefore difficult to distinguish from each other. Since these similar-behaving defects may have widely varying stability characteristics, those which are unstable over time pose a reliability problem. BIST can identify potentially unstable defects [13]. In addition, simultaneously existing multiple failure sources can cause misbehavior masking [12] that often leads to hard-to-detect defects because the misbehavior due to one defect is negated by that caused by another defect. BIST offers a way of detecting hard-to-detect defects [13]. Since the complexity and range of applications of MEMS have grown, off-chip testing has increased in cost, which in turn has enhanced the need for on-chip self-test capability. Current commercial BIST techniques are similar to the one described in [15] and commonly require calibration and therefore are not useful for manufacturing test. Hence, BIST suitable for man-

---

\*This research is sponsored by the National Science Foundation under grant MIP-9702678.

ufacturing test of MEMS is needed. Previous work [13]-[17] has addressed some of these problems. For example, our work [13, 18] describes a BIST approach that samples outputs from symmetrically-located nodes of the MEMS microstructure. Increasing observability in this way allows one to identify misbehavior resulting from local defects as opposed to more benign causes such as global etch variation.

The work in this paper is a continuation of the differential BIST approach [13, 18] and aims to build a mathematical model for an integrated and comprehensive approach to this form of BIST. In addition to self-test, our technique can be used for device and wafer characterization. Our analyses show that the BIST measurements can reveal significant information about the nature of local manufacturing variations affecting different portions of a given die.

The remaining portions of this paper are organized into the following sections. Section 2 describes a model of the capacitor-based sensing network used in a MEMS accelerometer. Section 3 describes the model developed for representing local manufacturing variations. Section 4 discusses the extent to which each BIST modulation scheme is sensitive to different types of local manufacturing variations. Finally, in section 5, conclusions are drawn based on how sensitive the various modes of BIST are to specific local manufacturing variations in the accelerometer sensor.

## 2 Capacitor Network Model

The MEMS device used in our analysis represents the most common inertial sensor, the standard spring-beam, electrostatic combdrive, single-axis, accelerometer [7]. A MEMS accelerometer is a transducer that converts translational acceleration to an electrical voltage signal. An accelerometer’s mechanical sensor (see Figure 1) can be viewed as a collection of primitive microstructures that include beams, anchors and a plate called the shuttle. Anchors attach beams to the substrate only at the positions shown in Figure 1. Beams that are anchored at one end and are connected to the shuttle at the other end, act as springs since they create a restoring force when the shuttle moves as a result of an acceleration. The remaining beams are typically referred to as “fingers”. Accelerometer fingers are partitioned into two classes: fixed and movable. Fixed fingers are anchored to the die surface and therefore cannot move. Movable fingers are attached to the shuttle and therefore move along with the shuttle. Subsets of fixed and movable fingers, called combdrives, also serve various purposes. The *sense* fingers enable measurement of shuttle movement in the *Y* direction while *actuation* fingers are used to create an electrostatic force that moves the shuttle for in-field testing purposes [15]. Note that the sensing is capacitive since a mechanical displacement of the shuttle is translated into a change in the voltage output from a capacitive voltage divider circuit formed by the air gaps between the fixed and movable fingers.

We have focussed on CMOS-MEMS [22] since the

MEMS can be easily integrated into a standard CMOS process. Moreover, the availability of multiple routing layers adds flexibility to BIST for CMOS-MEMS as compared to technologies where routability is limited. Figure 1 illustrates the topology of a CMOS-MEMS accelerometer sensor [23], which in this case is an example of a symmetric MEMS device. The sense operation is based on the fully differential sensing technique [22] and the sense signal is tapped from the sense combdrive capacitors.

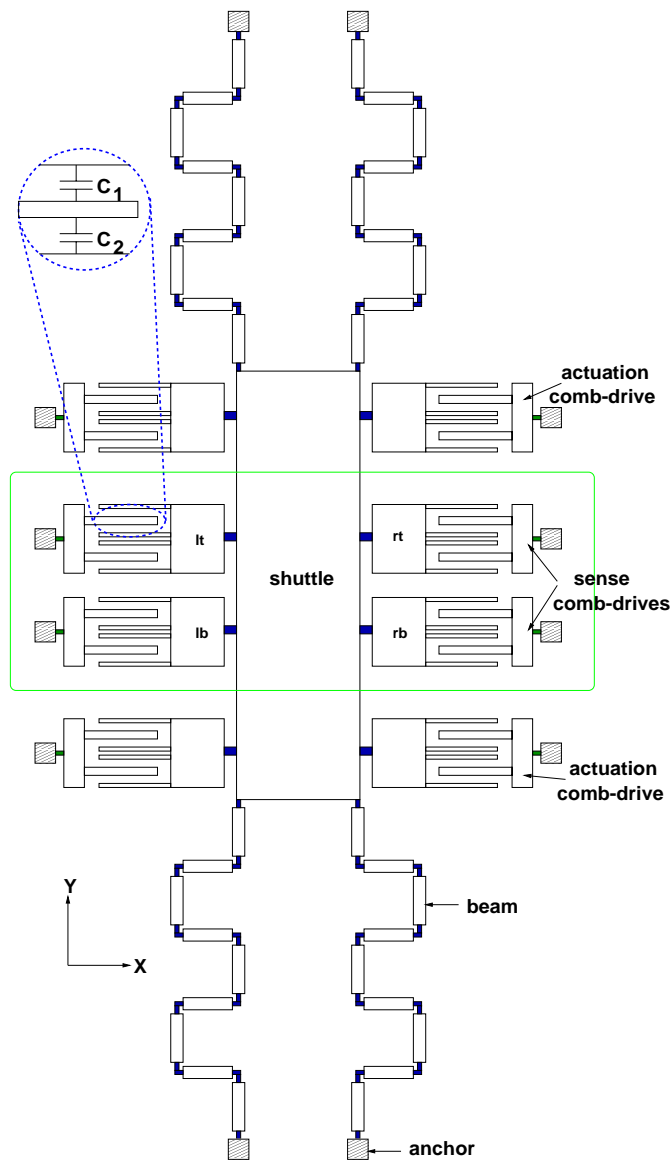


Figure 1: Topology of the accelerometer sensor.

As shown in Figure 1, the sensor has four identical, symmetrically-located sense combdrives. The circuit network constituted by the capacitors in the four sense combdrives is shown in Figure 2(a). The symbols ‘l’, ‘r’, ‘b’, and ‘t’ denote left, right, bottom and top, respectively. The symbols ‘l’

and ‘2’ denote the two capacitors of a differential pair within a combdrive. For shuttle motion in  $+Y$  direction, all capacitors with a subscript ‘1’ decrease while all capacitors with a subscript ‘2’ increase, and *vice-versa*.

## 2.1 Modulation Schemes

The capacitors in the sensor of Figure 1 can be represented by the equivalent network shown in Figure 2(a). The combdrive

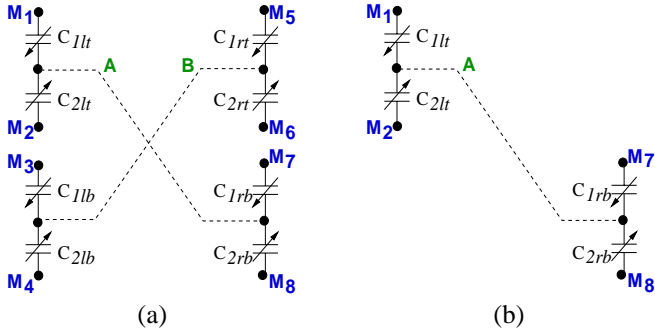


Figure 2: Network of capacitors representing the potential divider circuit formed by a set of sense combdrives in (a) the fully-differential sensing scheme and its simplified case, (b) the basic differential sensing scheme. Nodes  $A$  and  $B$  are sense nodes while  $M_1 - M_8$  are modulation nodes.

capacitors displayed in Figure 2 have the following characteristics:

1. Each pair of electrically-connected capacitors constitutes a potential divider circuit with potential being applied to each free or *modulation* node of each capacitor and voltage sensed from their common node or *sense* node. Thus, each capacitor pair has one sense node and two modulation nodes.
2. Each pair of capacitors must have different signals applied to their modulation nodes in order for the sense node to be sensitive to changes in the capacitances. Usually the modulation signals are applied in opposite phases. Therefore each capacitor pair can be considered a *dipole*<sup>1</sup>.
3. The number of modulation *states* associated with each dipole is given by the permutation  ${}^m P_2 = m(m-1)$ , where  $m$  is the number of phases of the applied modulation signal, or in general, the number of modulation signals. So, if one of  $m$  modulation signals is applied to one modulation node, then there is a choice of  $m-1$  signals for the other modulation node.

For  $m = 2$ , each dipole can have two possible states, denoted by the symbols 0 or 1. Every dipole has two capacitors, one labeled with a ‘1’ in the subscript and the other with a ‘2’ in

<sup>1</sup>A dipole is defined as an object with opposite polarities at its two ends.

the subscript. If the  $+$  phase ( $V_{mp}$ ) of the modulation signal is applied to the free node of the capacitor with subscript ‘1’, then the  $-$  phase ( $V_{mn}$ ) of the modulation signal, naturally, is applied to the free node of the capacitor with subscript ‘2’, and the dipole is said to be in state 0. Similarly, by swapping the modulation signals, the dipole is placed in state 1. A capacitor network consisting of  $n$  dipoles can be in  $2^n$  modes. However, changing the state of each dipole will only change the polarity of the sense output. Hence, only  $2^{n-1}$  modes need to be considered. This number can be further reduced since only the balanced modes (*i.e.*, modes with equal number of 0’s and 1’s) and the all-zero mode (or its mirror, the all-one mode) are interesting. This translates to a value of  $\frac{{}^n C_{n/2}}{2} + 1$ . For our case of  $n = 4$ , the number of modes is  $\frac{{}^4 C_2}{2} + 1 = 3 + 1 = 4$ .

## 2.2 Modal Dependence Relations

The sense outputs  $V_A$  and  $V_B$  (defined in Table 1) depend on changes in the capacitors of the electrical network shown in Figure 2(a). In the fully-differential sensing topology [23], the *change* in the voltage difference,  $V_B - V_A$ , is of most interest. Here, based on electrical network theory, we derive a relation that captures the dependence of  $V_B - V_A$  on changes in the network capacitances.

Based on the topology described in Figure 2(a) and the notation defined in Table 1, the total capacitance at nodes  $A$  and  $B$  are:

$$C_{A_{total}} = C_{1lt} + C_{2lt} + C_{1rb} + C_{2rb} + C_{pA} \quad (1)$$

$$C_{B_{total}} = C_{1lb} + C_{2lb} + C_{1rt} + C_{2rt} + C_{pB} \quad (2)$$

However, if the dipole capacitances ( $C_{ji}$ ) change (*e.g.*, due to shuttle displacement), then the corresponding altered values would be:

$$C'_{A_{total}} = C'_{1lt} + C'_{2lt} + C'_{1rb} + C'_{2rb} + C_{pA} \quad (3)$$

$$C'_{B_{total}} = C'_{1lb} + C'_{2lb} + C'_{1rt} + C'_{2rt} + C_{pB} \quad (4)$$

If we impose the condition that the sum of the capacitances in a dipole is *constant* (for small displacements), we have the following:

$$C_{1i} + C_{2i} = C'_{1i} + C'_{2i} \Rightarrow \Delta C_{1i} = -\Delta C_{2i}, \text{ where } i \in \{lt, rb, lb, rt\} \quad (5)$$

Substituting Equation 5 into Equations 1-4 leads to the conclusion that  $C_{A_{total}} = C'_{A_{total}}$  and  $C_{B_{total}} = C'_{B_{total}}$ . Hence, we have the following relations

$$\Delta V_A = \frac{\Delta C_{1lt}(V_{1lt} - V_{2lt}) + \Delta C_{1rb}(V_{1rb} - V_{2rb})}{C_{A_{total}}} \quad (6)$$

$$\Delta V_B = \frac{\Delta C_{1lb}(V_{1lb} - V_{2lb}) + \Delta C_{1rt}(V_{1rt} - V_{2rt})}{C_{B_{total}}} \quad (7)$$

As already mentioned, there are two phases of the modulation signal, namely  $V_{mp}$  and  $V_{mn}$ . Also, different phases of the modulation signal are applied to the two free nodes of each dipole. Hence, if  $V_{1lt} = V_{mp}, V_{2lt} = V_{mn}$ , then dipole  $lt$  is in state 0 ( $S_{lt} = 1$ ). On the other hand, if  $V_{1lt} = V_{mn}, V_{2lt} = V_{mp}$ ,

Symbol	Definition
$V_A, V_B$	Sense voltage output at nodes $A$ and $B$ (see Figure 2(a)), respectively.
$V_{mp}, V_{mn}$	Positive and negative phases of modulation signals, respectively.
$C_{pA}, C_{pB}$	Total parasitic capacitance to ground from sense nodes $A$ and $B$ , respectively. It includes amplifier input capacitance, interconnect capacitance, and values of all other capacitors connected (from non-sensing nodes) to the sense node.
$C_{A_{total}}, C_{B_{total}}$	Total capacitance at nodes $A$ and $B$ , respectively.
$C_{ji}$	Capacitance of a dipole capacitor (see Figure 2(a)), where $j \in \{1, 2\}$ and $i \in \{lt, rb, lb, rt\}$ .
$C'_{ji}$	Altered capacitance of a dipole capacitor, where $j \in \{1, 2\}$ and $i \in \{lt, rb, lb, rt\}$ .
$\Delta C_{ji}$	$C'_{ji} - C_{ji}$ , where $j \in \{1, 2\}$ and $i \in \{lt, rb, lb, rt\}$ .
$V_{ji}$	Voltage applied to modulation node of capacitor $C_{ji}$ (see Figure 2(a)), where $j \in \{1, 2\}$ and $i \in \{lt, rb, lb, rt\}$ .
$C_0$	Nominal capacitance of $C_{ji}$ , in absence of any local and global manufacturing variations.
$\delta$	Nominal capacitance change in $C_{ji}$ , in absence of any local and global manufacturing variations, for a typical shuttle displacement. Note that $ \delta/C_0  \leq 0.05$ for normal device operation.
$S_i$	A variable associated with dipole $i$ , where $i \in \{lt, rb, lb, rt\}$ . $S_i = 1$ , if dipole $i$ is in state 0 and $S_i = -1$ , if dipole $i$ is in state 1.
$\lambda_i$	Effective local manufacturing variation factor for the capacitance of dipole $i$ , where $i \in \{lt, rb, lb, rt\}$ . In absence of any manufacturing variations, $\lambda_i = 1$ . It is assumed to be constant for small displacements of the movable parts of the device.

Table 1: Model notation and definitions.

then dipole  $lt$  is in state 1 ( $S_{lt} = -1$ ). Similar reasoning applies for all other dipoles. Therefore, Equations 6 and 7 reduce to:

$$\Delta V_A = \frac{S_{lt}\Delta C_{1lt} + S_{rb}\Delta C_{1rb}}{C_{A_{total}}}(V_{mp} - V_{mn}) \quad (8)$$

$$\Delta V_B = \frac{S_{lb}\Delta C_{1lb} + S_{rt}\Delta C_{1rt}}{C_{B_{total}}}(V_{mp} - V_{mn}) \quad (9)$$

Subtracting Equation 8 from Equation 9, we get

$$\frac{\Delta V_B - \Delta V_A}{V_{mp} - V_{mn}} = \frac{S_{lb}\Delta C_{1lb} + S_{rt}\Delta C_{1rt}}{C_{B_{total}}} - \frac{S_{lt}\Delta C_{1lt} + S_{rb}\Delta C_{1rb}}{C_{A_{total}}} \quad (10)$$

Equation 10 is the *unified expression for all modes* for the network configuration illustrated in Figure 2(a).

Any one of Equations 6 or 7 is also applicable to basic differential sensing scheme used in devices manufactured from single-conductor processes such as MUMPS [24]. Since the basic differential case uses only one diagonal (e.g., the one with sense node A) of the network in Figure 2(a), it is reduced to that shown in Figure 2(b). The change in voltage of the sense node  $A$  is obtained by substituting  $V_{1lt} = V_{mp}$ ,  $V_{1rb} = V_{mn}$ , and  $V_{2lt} = V_{2rb} = \frac{V_{mp} + V_{mn}}{2}$  in Equation 6, which then reduces to:

$$\frac{\Delta V_A}{V_{mp} - V_{mn}} = \frac{\Delta C_{1lt} - \Delta C_{1rb}}{2C_{A_{total}}}$$

### 3 Local Manufacturing Variations

Combdrive capacitance (same as dipole capacitance  $C_{ji}$ ) depends on physical parameters such as finger width, the gap between fingers, finger thickness, relative combdrive height difference, etc. All of these parameters may vary over the plane of the device, meaning each is a function of location. In our analyses, each point in the device layout is represented by the coordinates  $(\alpha, \beta)$ . Here, we analyze the combined effect of all

local manufacturing variations on a dependent variable (e.g., combdrive capacitance) distributed over device area  $A$ . The dimensionless variable  $\lambda(\alpha, \beta)$  represents local manufacturing variations and its impact on combdrive capacitance is characterized as:

$$C_{ji} = C_0 \int_A \lambda(\alpha, \beta) \frac{d\alpha d\beta}{A} \quad (11)$$

In the absence of local manufacturing variations,  $\lambda(\alpha, \beta) = 1, \forall \alpha, \forall \beta$ , and Equation 11 reduces to the simple relation,  $C_{ji} = C_0$ . Hence,  $C_0$  is the nominal value of  $C_{ji}$ .

Next, we assume that  $\lambda(\alpha, \beta)$  is *variable separable*<sup>2</sup>, that is,

$$\lambda(\alpha, \beta) = [1 + X(\alpha)][1 + Y(\beta)] \quad (12)$$

where  $X(\alpha)$  and  $Y(\beta)$  are functions of  $\alpha$  only and  $\beta$  only, respectively. This implies that manufacturing variations along the  $X$  and  $Y$  axes are independent of each other. From Equation 12, it is evident that the condition  $X(\alpha) = Y(\beta) = 0, \forall \alpha, \forall \beta$ , implies no local variation. The functions  $X(\alpha)$  and  $Y(\beta)$  are subject to these conditions:  $-1 < X(\alpha), -1 < Y(\beta)$ ,  $X(0) = Y(0) = 0$ . Note that  $(\alpha, \beta) = (0, 0)$  at the center of the layout. Substituting Equation 12 into Equation 11 gives the following expression for  $C_{ji}$ .

$$\begin{aligned} C_{ji} &= C_0 \int_A [1 + X(\alpha)][1 + Y(\beta)] \frac{d\alpha d\beta}{A}, \text{ where } A = (\alpha_2 - \alpha_1)(\beta_2 - \beta_1) \\ &= C_0 \int_{\alpha_1}^{\alpha_2} [1 + X(\alpha)] \frac{d\alpha}{\alpha_2 - \alpha_1} \int_{\beta_1}^{\beta_2} [1 + Y(\beta)] \frac{d\beta}{\beta_2 - \beta_1} \\ &= C_0 [1 + \bar{X}] [1 + \bar{Y}] \end{aligned} \quad (13)$$

Using the Mean Value Theorem of differential calculus, it can

<sup>2</sup>A function  $f(x, y)$  is said to be variable separable if it can be expressed as a product of two functions  $f_1$  and  $f_2$  such that  $f_1$  is a function of  $x$  alone and  $f_2$  is a function of  $y$  alone.

be shown that there exists a location  $(\alpha_0, \beta_0)$  in area  $A$  such that  $X(\alpha_0) = \bar{X}$  and  $Y(\beta_0) = \bar{Y}$ . Substituting  $\bar{X} = X(\alpha_0)$  and  $\bar{Y} = Y(\beta_0)$  into Equation 13 gives:

$$\begin{aligned} C_{ji} &= C_0[1 + \bar{X}][1 + \bar{Y}] = C_0[1 + X(\alpha_0)][1 + Y(\beta_0)] \\ &= C_0\lambda(\alpha_0, \beta_0) \end{aligned} \quad (14)$$

Equation 14 captures the concept of average manufacturing variations. Since the capacitance is distributed over an area, the combined effect of all manufacturing variations over the area is equated to an average multiplied by the same area. Hence, we will use these average values to represent combdrive capacitances.

Equation 14 indicates that the average manufacturing variation in a quadrant can be represented by the value of  $\lambda$  at a single point in the quadrant. Therefore, the point locations  $(\alpha^+, \beta^+)$  and  $(\alpha^-, \beta^-)$  are assigned to the combdrives in two diagonally opposite quadrants, right-top ( $rt$ ) and left-bottom ( $lb$ ), respectively. We can now have the following relations for these two quadrants:

$$\begin{aligned} \frac{C_{1rt}}{C_0} &= \frac{C_{2rt}}{C_0} = \lambda_{rt} = \lambda(\alpha^+, \beta^+) = [1 + X(\alpha^+)][1 + Y(\beta^+)] \\ &= \int_{\alpha_1}^{\alpha_2} [1 + X(\alpha)] \frac{d\alpha}{\alpha_2 - \alpha_1} \int_{\beta_1}^{\beta_2} [1 + Y(\beta)] \frac{d\beta}{\beta_2 - \beta_1} \end{aligned} \quad (15)$$

$$\begin{aligned} \frac{C_{1lb}}{C_0} &= \frac{C_{2lb}}{C_0} = \lambda_{lb} = \lambda(\alpha^-, \beta^-) = [1 + X(\alpha^-)][1 + Y(\beta^-)] \\ &= \int_{-\alpha_2}^{-\alpha_1} [1 + X(\alpha)] \frac{d\alpha}{\alpha_2 - \alpha_1} \int_{-\beta_2}^{-\beta_1} [1 + Y(\beta)] \frac{d\beta}{\beta_2 - \beta_1} \end{aligned} \quad (16)$$

It follows from Equations 15 and 16 that for the combdrives in the other two quadrants, left-top ( $lt$ ) and right-bottom ( $rb$ ):

$$\begin{aligned} \frac{C_{1lt}}{C_0} &= \frac{C_{2lt}}{C_0} = \lambda_{lt} = \lambda(\alpha^-, \beta^+) = [1 + X(\alpha^-)][1 + Y(\beta^+)] \\ &= \int_{-\alpha_2}^{-\alpha_1} [1 + X(\alpha)] \frac{d\alpha}{\alpha_2 - \alpha_1} \int_{\beta_1}^{\beta_2} [1 + Y(\beta)] \frac{d\beta}{\beta_2 - \beta_1} \end{aligned} \quad (17)$$

$$\begin{aligned} \frac{C_{1rb}}{C_0} &= \frac{C_{2rb}}{C_0} = \lambda_{rb} = \lambda(\alpha^+, \beta^-) = [1 + X(\alpha^+)][1 + Y(\beta^-)] \\ &= \int_{\alpha_1}^{\alpha_2} [1 + X(\alpha)] \frac{d\alpha}{\alpha_2 - \alpha_1} \int_{-\beta_2}^{-\beta_1} [1 + Y(\beta)] \frac{d\beta}{\beta_2 - \beta_1} \end{aligned} \quad (18)$$

Equations 15-18 show how the combdrive capacitance in each of the four quadrants depends on average local manufacturing variations.

## 4 Mode Sensitivity

Here, we analyze how the sense combdrive capacitors, under different modulation schemes, produce a sense signal that may or may not depend on first-order<sup>3</sup> local manufacturing variations, device rotation, DC offset, and combdrive connectivity.

<sup>3</sup>The first-order dependence of variable  $y$  on variable  $x$  is  $\left[\frac{dy}{dx}\right]_{x=0}$ .

## 4.1 Manufacturing Variations

In the presence of manufacturing variations, the dipole capacitors (same as combdrive capacitors) have these values for zero shuttle displacement:

$$C_{ji} = C_0\lambda_i, \text{ where } i \in \{rt, lb, lt, rb\}, j \in \{1, 2\} \quad (19)$$

When the shuttle is displaced, the expressions for the combdrive capacitors change to:

$$C'_{1i} = (C_0 - \delta)\lambda_i, \text{ where } i \in \{rt, lb, lt, rb\} \quad (20)$$

$$C'_{2i} = (C_0 + \delta)\lambda_i, \text{ where } i \in \{rt, lb, lt, rb\} \quad (21)$$

Based on the definitions in Table 1 and Equation 20, we have  $\Delta C_{1lt} = -\delta\lambda_{lt}$ ,  $\Delta C_{1rb} = -\delta\lambda_{rb}$ ,  $\Delta C_{1lb} = -\delta\lambda_{lb}$ ,  $\Delta C_{1rt} = -\delta\lambda_{rt}$ ,  $C_{A_{total}} = 2C_0(\lambda_{lt} + \lambda_{rb}) + C_{pA}$ , and  $C_{B_{total}} = 2C_0(\lambda_{lb} + \lambda_{rt}) + C_{pB}$ . Substituting these values in Equation 10 gives

$$\begin{aligned} \frac{\Delta V_B - \Delta V_A}{V_{mp} - V_{mn}} &= \delta \left[ \frac{S_{lt}\lambda_{lt} + S_{rb}\lambda_{rb}}{2C_0(\lambda_{lt} + \lambda_{rb}) + C_{pA}} - \frac{S_{lb}\lambda_{lb} + S_{rt}\lambda_{rt}}{2C_0(\lambda_{lb} + \lambda_{rt}) + C_{pB}} \right] \\ &= \delta \cdot F(S_{lt}, S_{rb}, S_{lb}, S_{rt}) \end{aligned} \quad (22)$$

where  $F$  is given by

$$F(x_1, x_2, x_3, x_4) = \frac{x_1\lambda_{lt} + x_2\lambda_{rb}}{2C_0(\lambda_{lt} + \lambda_{rb}) + C_{pA}} - \frac{x_3\lambda_{lb} + x_4\lambda_{rt}}{2C_0(\lambda_{lb} + \lambda_{rt}) + C_{pB}} \quad (24)$$

Equation 22 allows us to represent the modes of the capacitive network (shown in Figure 2(a)) in the form of a truth table in Table 2. Every row in Table 2 corresponds to a mode of the capacitive network. For example, the fourth row is for mode 0000.

For simplicity, we assume equal parasitic capacitance, *i.e.*,  $C_{pA} = C_{pB} = C_p$ . In addition, for the sake of convenience, we define the following quantities:

$$\mu = \frac{C_p}{4C_0} \quad (25)$$

$$X_s = X(\alpha^+) + X(\alpha^-), \quad Y_s = Y(\beta^+) + Y(\beta^-) \quad (26)$$

$$X_d = X(\alpha^+) - X(\alpha^-), \quad Y_d = Y(\beta^+) - Y(\beta^-) \quad (27)$$

$$H(X_s, Y_s, X_d, Y_d) = - \left[ \frac{X_d Y_d}{2} \right]^2 + \left[ 2\mu + \frac{(2 + X_s)(2 + Y_s)}{2} \right]^2 \quad (28)$$

Substituting Equations 15-18 into Equation 22 and then simplifying with the expressions of Equations 25-28 gives the differential sense output for various modes as tabulated in Table 3.

From Equation 26, it is clear that  $X_s = Y_s = 0$  when  $X(\alpha)$  and  $Y(\beta)$  are *odd*<sup>4</sup> functions. Also,  $X_d$  and  $Y_d$  (defined in Equation 27) are much smaller than unity for a normal manufacturing process so that  $\left(\frac{X_d Y_d}{4}\right)^2 \ll 1$ . Under such conditions, the expressions of mode sensitivities in Table 3 reduce to the ones listed in Table 4. Table 4 reveals how local manufacturing variations affect various mode sensitivities and how modes can be

<sup>4</sup> $f(x)$  is said to be an odd function of  $x$  if  $f(-x) = -f(x)$ .

Mode ( <i>lt.rb.lb.rt</i> )	Dipole states				Normalized sense output $= (\Delta V_B - \Delta V_A) / (V_{mp} - V_{mn})$	Mode name
	$C_{1lt} : C_{2lt}$	$C_{1rb} : C_{2rb}$	$C_{1lb} : C_{2lb}$	$C_{1rt} : C_{2rt}$		
0011	0	0	1	1	$\delta \frac{\lambda_{lt} + \lambda_{rb}}{2C_0(\lambda_{lt} + \lambda_{rb}) + C_{pA}} + \delta \frac{\lambda_{lb} + \lambda_{rt}}{2C_0(\lambda_{lb} + \lambda_{rt}) + C_{pB}}$	Normal sense mode
0110	0	1	1	0	$\delta \frac{\lambda_{lt} - \lambda_{rb}}{2C_0(\lambda_{lt} + \lambda_{rb}) + C_{pA}} + \delta \frac{\lambda_{lb} - \lambda_{rt}}{2C_0(\lambda_{lb} + \lambda_{rt}) + C_{pB}}$	Self-test X-mode
0101	0	1	0	1	$\delta \frac{\lambda_{lt} - \lambda_{rb}}{2C_0(\lambda_{lt} + \lambda_{rb}) + C_{pA}} - \delta \frac{\lambda_{lb} - \lambda_{rt}}{2C_0(\lambda_{lb} + \lambda_{rt}) + C_{pB}}$	Self-test Y-mode
0000	0	0	0	0	$\delta \frac{\lambda_{lt} + \lambda_{rb}}{2C_0(\lambda_{lt} + \lambda_{rb}) + C_{pA}} - \delta \frac{\lambda_{lb} + \lambda_{rt}}{2C_0(\lambda_{lb} + \lambda_{rt}) + C_{pB}}$	Self-test XY-mode

Table 2: Expressions for sense output voltage of various modes of the capacitive network in presence of local manufacturing variations.

Mode ( <i>lt.rb.lb.rt</i> )	Normalized sense output $= (\Delta V_B - \Delta V_A) / (V_{mp} - V_{mn})$
0011	$\frac{\delta}{C_0} \left[ 1 - \mu \cdot \frac{(2+X_s)(2+Y_s)+4\mu}{H(X_s, Y_s, X_d, Y_d)} \right]$
0110	$\frac{\delta}{2C_0} (-X_d) \left[ \frac{2\{1+Y_s+Y(\beta^+)Y(\beta^-)\}(2+X_s)+2\mu Y_s+4\mu}{H(X_s, Y_s, X_d, Y_d)} \right]$
0101	$\frac{\delta}{2C_0} (+Y_d) \left[ \frac{2\{1+X_s+X(\alpha^+)X(\alpha^-)\}(2+Y_s)+2\mu X_s+4\mu}{H(X_s, Y_s, X_d, Y_d)} \right]$
0000	$\frac{\delta}{2C_0} (-X_d Y_d) \left[ \frac{2\mu}{H(X_s, Y_s, X_d, Y_d)} \right]$

Table 3: Changes in sense voltage outputs for various modes of accelerometer operation.

used to estimate manufacturing variations along specific directions in the device layout.

## 4.2 Rotation

In-plane rotation of the device causes the capacitors in diagonally-located combs to either increase or decrease. For example, if  $C_{lb}$  and  $C_{rt}$  increase,  $C_{lt}$  and  $C_{rb}$  will decrease. If the change in capacitance of one combdrive due to rotation alone is  $\delta_{rot}$ , from Equations 8 and 9, we have these sense voltages in presence of both translation and rotation:

$$\Delta V_A = -(\delta + \delta_{rot}) \frac{S_{lt}\lambda_{lt} + S_{rb}\lambda_{rb}}{2C_0(\lambda_{lt} + \lambda_{rb}) + C_{pA}} (V_{mp} - V_{mn}) \quad (29)$$

$$\Delta V_B = -(\delta - \delta_{rot}) \frac{S_{lb}\lambda_{lb} + S_{rt}\lambda_{rt}}{2C_0(\lambda_{lb} + \lambda_{rt}) + C_{pB}} (V_{mp} - V_{mn}) \quad (30)$$

Combining Equations 29 and 30, we have:

$$\begin{aligned} & \frac{\Delta V_B - \Delta V_A}{V_{mp} - V_{mn}} \\ &= (\delta + \delta_{rot}) \frac{S_{lt}\lambda_{lt} + S_{rb}\lambda_{rb}}{2C_0(\lambda_{lt} + \lambda_{rb}) + C_{pA}} - (\delta - \delta_{rot}) \frac{S_{lb}\lambda_{lb} + S_{rt}\lambda_{rt}}{2C_0(\lambda_{lb} + \lambda_{rt}) + C_{pB}} \\ &= \delta \left[ \frac{S_{lt}\lambda_{lt} + S_{rb}\lambda_{rb}}{2C_0(\lambda_{lt} + \lambda_{rb}) + C_{pA}} - \frac{S_{lb}\lambda_{lb} + S_{rt}\lambda_{rt}}{2C_0(\lambda_{lb} + \lambda_{rt}) + C_{pB}} \right] \\ &+ \delta_{rot} \left[ \frac{S_{lt}\lambda_{lt} + S_{rb}\lambda_{rb}}{2C_0(\lambda_{lt} + \lambda_{rb}) + C_{pA}} + \frac{S_{lb}\lambda_{lb} + S_{rt}\lambda_{rt}}{2C_0(\lambda_{lb} + \lambda_{rt}) + C_{pB}} \right] \quad (31) \end{aligned}$$

Using Equation 24, Equation 31 can be represented as

$$\frac{\Delta V_B - \Delta V_A}{V_{mp} - V_{mn}} = \delta \cdot F(S_{lt}, S_{rb}, S_{lb}, S_{rt}) + \delta_{rot} \cdot F(S_{lt}, S_{rb}, -S_{lb}, -S_{rt}) \quad (32)$$

Equation 32 reveals that this is a mixed-mode case, which is equivalent to two different modes being active simultaneously. Basically, if the externally applied mode is  $M = abcd$ , an internally generated mode due to rotation will be  $M_{rot} = ab\bar{c}\bar{d}$  or  $M_{rot} = \bar{a}\bar{b}cd$ . Hence, the combined effect is a linear superposition of modes,  $M + M_{rot}$ . The two modes may reinforce each other or oppose each other, depending on their relative magnitudes and signs. Thus, the effect of in-plane rotation can be captured by using the principle of linear superposition.

Out-of-plane rotation/curvature usually causes all comb capacitances involved to decrease. Hence, it can be modeled as any other manufacturing variation.

## 4.3 DC-offset

Equation 22 was derived with the assumption that the change in combdrive capacitance, in absence of any local manufacturing variations, is the same for all sense combdrives. It is, however, independent of how the capacitances are changed. Since we can reasonably assume that the capacitance change due to a DC-offset is the same for all sense combdrives, Equation 22 remains applicable.

## 4.4 Different Network Configurations

Our previous analyses are applicable to a specific type of configuration, where combdrive pairs (see Figure 2(a)) are electrically connected diagonally ([lb,rt] and [lt,rb]). Alternative configurations of the capacitor network are also possible, such as horizontal ([lb,rb] and [lt,rt]) and vertical ([lb,lt] and [rb,rt]) connectivity. Table 5 lists the sensitivities for selected modes

Mode ( <i>lt.rb.lb.rt</i> )	Normalized sense output = $(\Delta V_B - \Delta V_A)/(V_{mp} - V_{mn})$	Dependence
0011	$\frac{\delta}{C_0} \left[ \frac{1}{1 + \frac{C_p}{4C_0}} \right]$	Independent of X and Y variations
0110	$\frac{\delta}{2C_0} (-X_d) \left[ \frac{1 + \frac{C_p}{4C_0} + Y(\beta^+)Y(\beta^-)}{(1 + \frac{C_p}{4C_0})^2} \right]$	Dependent on X variations only (to 1st order)
0101	$\frac{\delta}{2C_0} (+Y_d) \left[ \frac{1 + \frac{C_p}{4C_0} + X(\alpha^+)X(\alpha^-)}{(1 + \frac{C_p}{4C_0})^2} \right]$	Dependent on Y variations only (to 1st order)
0000	$\frac{\delta}{4C_0} (-X_d Y_d) \left[ \frac{\frac{C_p}{4C_0}}{(1 + \frac{C_p}{4C_0})^2} \right]$	Dependent on both X and Y variations

Table 4: Changes in sense voltage outputs for various modes of accelerometer operation (in diagonal configuration) and their relationship to specific types of manufacturing variations.

Mode ( <i>lt.rb.lb.rt</i> )	Normalized sense output = $(\Delta V_B - \Delta V_A)/(V_{mp} - V_{mn})$	
	Horizontal connectivity	Vertical connectivity
0011	$\delta \frac{\lambda_{lb} - \lambda_{rb}}{2C_0(\lambda_{lb} + \lambda_{rb}) + C_p} + \delta \frac{\lambda_{lt} - \lambda_{rt}}{2C_0(\lambda_{lt} + \lambda_{rt}) + C_p}$	$\delta \frac{-\lambda_{lb} + \lambda_{lt}}{2C_0(\lambda_{rb} + \lambda_{lt}) + C_p} - \delta \frac{\lambda_{rb} - \lambda_{rt}}{2C_0(\lambda_{rb} + \lambda_{rt}) + C_p}$
0110	$\delta \frac{\lambda_{lb} + \lambda_{rb}}{2C_0(\lambda_{lb} + \lambda_{rb}) + C_p} + \delta \frac{\lambda_{lt} + \lambda_{rt}}{2C_0(\lambda_{lt} + \lambda_{rt}) + C_p}$	$\delta \frac{-\lambda_{lb} + \lambda_{lt}}{2C_0(\lambda_{rb} + \lambda_{lt}) + C_p} + \delta \frac{\lambda_{rb} - \lambda_{rt}}{2C_0(\lambda_{rb} + \lambda_{rt}) + C_p}$
0101	$\delta \frac{-\lambda_{lb} + \lambda_{rb}}{2C_0(\lambda_{lb} + \lambda_{rb}) + C_p} + \delta \frac{\lambda_{lt} - \lambda_{rt}}{2C_0(\lambda_{lt} + \lambda_{rt}) + C_p}$	$\delta \frac{\lambda_{lb} + \lambda_{lt}}{2C_0(\lambda_{rb} + \lambda_{lt}) + C_p} + \delta \frac{\lambda_{rb} + \lambda_{rt}}{2C_0(\lambda_{rb} + \lambda_{rt}) + C_p}$
0000	$-\delta \frac{\lambda_{lb} + \lambda_{rb}}{2C_0(\lambda_{lb} + \lambda_{rb}) + C_p} + \delta \frac{\lambda_{lt} + \lambda_{rt}}{2C_0(\lambda_{lt} + \lambda_{rt}) + C_p}$	$\delta \frac{\lambda_{lb} + \lambda_{lt}}{2C_0(\lambda_{rb} + \lambda_{lt}) + C_p} - \delta \frac{\lambda_{rb} + \lambda_{rt}}{2C_0(\lambda_{rb} + \lambda_{rt}) + C_p}$

Table 5: Mode sensitivities for different configurations.

for these alternative configurations. Based on the expressions in Table 5, Table 6 lists how specific modes are sensitive or immune to certain types of local manufacturing variations under a particular configuration. Column 1 lists the type of capacitor network connectivity. Columns 2 and 3 list the type of variation (odd or even) along the  $X$  and  $Y$  directions, respectively. The remaining four columns list the sensitivity of four modes to the particular type of variation. Note that ‘1X’ (‘1Y’) implies a strong first order dependence on local manufacturing variation along the  $X$  ( $Y$ ) axis. Similarly, ‘1XY’ implies dependence on the product of local manufacturing variations along the  $X$  and  $Y$  axes. Note that ‘0.1’ has been used to imply a weak dependence on the corresponding variable while ‘1’ implies a strong dependence. Note that the entries in Table 6 only indicate a certain level of dependence on local manufacturing variations and not the exact magnitude. Below we describe some of the more interesting configurations.

1. For horizontal connectivity, in the presence of odd variations along both the  $X$  and  $Y$  axes, mode 0011 is sensitive to variation along the  $X$  axis only.
2. For diagonal connectivity, in the presence of odd variations along the  $X$  axis, mode 0110 is sensitive to variations along the  $X$  axis only.
3. For horizontal connectivity, in the presence of odd variations along the  $Y$  axis, mode 0000 is sensitive to variations along the  $Y$  axis only.

4. For diagonal connectivity, in the presence of even variations along the  $Y$  axis and odd variations along the  $X$  axis, mode 0011 is weakly sensitive to variations along the  $Y$  axis only.

In the following, we give examples of how sensitive various modes are to particular instances of local manufacturing variations, namely, etch variation. Note that over-etch and under-etch are arbitrarily assigned positive and negative polarities, respectively.

1. For a diagonal configuration and linear etch variation (an odd variation) along the  $X$  axis, the 0011 mode is much less sensitive than the 0110 mode. Simulation results (see rows 1-3 in Table 7) show that the absolute change in voltage output of the 0110 mode is about 1.5 times that of the 0011 mode. In fact, the relative change in the voltage output of the 0011 mode is only  $\pm 2.4\%$  while the relative change in the voltage output of the 0110 mode is several orders of magnitude. Incidentally, the sense output for mode 0101 is practically zero as expected (see rows 2-3 in Table 7).
2. For a diagonal configuration, if there are identical linear etch variations along the  $X$  and  $Y$  axes, modes 0110 and 0101 should produce outputs of the same magnitude. This is confirmed by row 4 in Table 7. As expected, the output for mode 0011 is practically unchanged (see rows 1 and 4 in Table 7).

Combdrive connectivity	Variation type		Modes ( <i>lt.rb.lb.rt</i> )			
	X axis	Y axis	0011	0110	0101	0000
Diagonal	Odd	Odd	0	1X	1Y	1XY
	Odd	Even	0.1Y	1X	0	0
	Even	Odd	0.1X	0	1Y	0
	Even	Even	0.1(X+Y)	0	0	0
Horizontal	Odd	Odd	1X	0	1XY	1Y
	Odd	Even	1X	0.1Y	0	0
	Even	Odd	0	0.1X	0	1Y
	Even	Even	0	0.1(X+Y)	0	0
Vertical	Odd	Odd	1Y	1XY	0	1X
	Odd	Even	0	0	0.1Y	1X
	Even	Odd	1Y	0	0.1X	0
	Even	Even	0	0	0.1(X+Y)	0

Table 6: Mode sensitivities under different types of local manufacturing variations and for different configurations.

Combdrive connectivity	Average etch variation in a quadrant (nm)				Resonant frequency (kHz)	Sense output for a mode = $\Delta V_B - \Delta V_A$ (V)			
	<i>lt</i>	<i>rb</i>	<i>lb</i>	<i>rt</i>		0011	0110	0101	0000
Diagonal	0	0	0	0	5.58	34.37m ( $\pm 0\%$ )	0	0	0
Diagonal	0	+25	0	+25	5.49	33.68m (-2.0%)	1.08m	-5.7p	179p
Diagonal	0	-25	0	-25	5.65	35.18m (+2.4%)	-1.17m	6.5p	-196p
Diagonal	0	0	+25	-25	5.57	34.47m (+0.3%)	-1.13m	1.13m	-46 $\mu$
Horizontal	+25	0	0	+25	5.49	0	33.70m	0	0.84m
Vertical	+25	0	0	+25	5.49	1.08m	0	33.71m	0

Table 7: Test outputs of various modes for etch variations across the sensor.

- For a diagonal configuration, mode 0000 is expected to give significant output only when there are odd variations along both  $X$  and  $Y$  axes. This is evident from Table 7 where the output of mode 0000 is negligible in rows 2-3 but significant in row 4.
- It can be shown that mode 0011 in the vertical configuration is more sensitive to a linear etch variation along the  $Y$  axis than mode 0000 in the horizontal configuration. This is confirmed by rows 5-6 of Table 7 which show the output of mode 0011 in the vertical configuration to be about 29% more than the output of mode 0000 in the horizontal configuration.

In fact, for every variation type listed in Table 6, it is possible to determine which mode under which network configuration is most sensitive. Thus, it is possible to select a minimal set of modes (and network configurations) that can capture the same information that all four modes under each of the three network configurations together can capture.

In order to characterize the device, a measurement from a BIST mode (say, diagonal mode 0110 in Table 4) can be translated to a value for the parameter  $X_d$ , which is a function of  $\alpha$  alone. In the ideal case (no local variations),  $X_d$  will be

found to be zero. The larger the value of  $X_d$ , the larger the mismatch between the left and right halves of the device, which is a measure of the amount of local variation along the  $X$  axis. Similarly, a measurement from the diagonal mode 0101 (see Table 4) can provide a value of  $Y_d$  which will indicate the mismatch between the lower and upper halves of the device, *i.e.*, a measure of the amount of local variation along the  $Y$  axis. Combining the two measurements using Equation 14 gives an estimate of  $\lambda$  for the combdrive capacitance in that quadrant. In this way, measures of the average local manufacturing variations for all quadrants ( $\lambda_{lt}, \lambda_{rb}, \lambda_{rt}, \lambda_{lb}$ ) of the device can be obtained.

Wafer characterization is an extension of device characterization, since collection of data from multiple dice (one die may have one or more devices) will give an estimate of how the  $\lambda$  parameter changes values across the wafer. Basically, a discrete two-dimensional plot of  $\lambda$  over the entire wafer can be used as a measure of manufacturing variations over the wafer.

## 5 Conclusions

Our model, when applied to the accelerometer sensor, shows that the differential self-test method [13, 18] is a very broad and versatile technique that can also be used for characterization, if appropriate modulation schemes are implemented. De-

vice characterization can be accomplished if the dependence of sense capacitances on local manufacturing variations is known. The electrical sensitivities measured from the various BIST modes can then be mapped into values of equivalent local manufacturing variations. While this work focuses on developing a theoretical model alone, simulation results validate the model's predictions. The current mathematical model explores a large space and now enables customization for characterization of specific types of manufacturing variations. The model is a generic one and can be easily applied to a device with any number of sub-parts that are identical by design, as described in [18].

## References

- [1] J. A. Walraven, "Introduction to Applications and Industries for Microelectromechanical Systems (MEMS)," *Proc. of International Test Conference*, pp. 674-680, Oct. 2003.
- [2] A. Kourepenis, J. Borenstein, J. Connelly, R. Elliott, P. Ward, and M. Weinberg, "Performance of MEMS Inertial Sensors," *Position Location and Navigation Symposium*, pp. 1-8, April 1998.
- [3] R. Lal, P. R. Apte, N. K. Bhat, G. Bose, S. Chandra, and D. K. Sharma, "MEMS: Technology, Design, CAD and Applications," *Proc. of Design Automation Conference*, pp. 24-25, Jan. 2002.
- [4] S. Cass, "MEMS in Space," *IEEE Spectrum*, Vol. 38, Issue 7, pp. 56-61, July 2001.
- [5] T. A. Lober and R. T. Howe, "Surface-micromachining Processes for Electrostatic Microactuator Fabrication," *IEEE Solid-State Sensor and Actuator Workshop, Technical Digest*, pp. 59-62, June 1988.
- [6] D. C. Hutchison, K. Ohara, and A. Takeda, "Application of Second Generation Advanced Multimedia Display Processor (AMDP2) in a Digital Micro-mirror Array based HDTV," *International Conference on Consumer Electronics (ICCE)*, pp. 294-295, June 2001.
- [7] R. S. Payne, S. Sherman, S. Lewis, and R. T. Howe, "Surface Micromachining: From Vision to Reality to Vision (accelerometer)," *Proc. of International Solid State Circuits Conference*, pp. 164-165, Feb. 1995.
- [8] R. Oboe, "Use of MEMS based Accelerometers in Hard Disk Drives," *Proc. of International Conference on Advanced Intelligent Mechatronics*, Vol. 2, pp. 1142-1147, 2001.
- [9] T. Jiang and R. D. Blanton, "Particulate Failures for Surface-Micromachined MEMS," *Proc. of International Test Conference*, pp. 329-337, Sept. 1999.
- [10] A. Hartzell and D. Woodilla, "Reliability Methodology for Prediction of Micromachined Accelerometer Stiction," *Proc. of Reliability Physics Symposium*, pp. 202-205, March 1999.
- [11] A. Kolpekwar, R. D. Blanton, and D. Woodilla, "Failure Modes for Stiction in Surface-Micromachined MEMS," *Proc. of International Test Conference*, pp. 551-556, Oct. 1998.
- [12] N. Deb and R. D. Blanton, "Analysis of Failure Sources in Surface-Micromachined MEMS," *Proc. of International Test Conference*, pp. 739-749, Oct. 2000.
- [13] N. Deb and R. D. Blanton, "Built-In Self-Test of CMOS-MEMS Accelerometers," *Proc. of International Test Conference*, pp. 1075-1084, Oct. 2002.
- [14] D. De Bruyker, A. Cozma, and R. Puers, "A Combined Piezoresistive/Capacitive Pressure Sensor with Self-test Function based on Thermal Actuation," *Proc. of Solid State Sensors and Actuators*, Vol. 2, pp. 1461-1464, 1997.
- [15] H.V. Allen, S.C. Terry, and D.W. de Bruin, "Self-Testable Accelerometer Systems," *Proc. of Micro Electro Mechanical Systems*, pp. 113-115, 1989.
- [16] B. Charlot, S. Mir, F. Parrain, and B. Courtois, "Electrically Induced Stimuli for MEMS Self-Test," *Proc. of VLSI Test Symposium*, pp. 210-215, Apr.-May 2001.
- [17] R. Rosing, A. Lechner, A. Richardson, and A. Dorey, "Fault Simulation and Modelling of Microelectromechanical Systems," *Computing and Control Engineering Journal*, Vol. 11, Issue 5, pp. 242-250, Oct. 2000.
- [18] N. Deb and R. D. Blanton, *U. S. Patent Pending, Application No. 10/666,147*, Filed Sept. 18, 2002.
- [19] W. C. Tang, T.-C. H. Nguyen, M. W. Judy, and R. T. Howe, "Electrostatic Comb Drive of Lateral Polysilicon Resonators," *Sensors and Actuators A*, Vol. 21, Nos. 1-3, pp. 328-331, Feb. 1990.
- [20] J. Xuesong, J. I. Seeger, M. Kraft, and B. E. Boser, "A Monolithic Surface Micromachined Z-axis Gyroscope with Digital Output," *Symposium on VLSI Circuits*, pp. 16-19, 2000.
- [21] N. Deb and R. D. Blanton, "High-Level Fault Modeling in Surface-Micromachined MEMS," *Proc. of Design, Test, Integration, and Packaging of MEMS/MOEMS*, pp. 228-235, May 2000.
- [22] H. Luo, G. K. Fedder, and L. R. Carley, "A 1 mG Lateral CMOS-MEMS Accelerometer," *Proc. of Micro Electro Mechanical Systems*, pp. 502-507, Jan. 2000.
- [23] J. Wu, G. K. Fedder, and L. R. Carley, "A Low-Noise Low-Offset Chopper-Stabilized Capacitive-readout Amplifier for CMOS MEMS Accelerometers," *Proc. of International Solid State Circuits Conference*, pp. 428-429, Feb. 2002.
- [24] D. A. Koester, R. Mahadevan, and K. W. Markus, *MUMPS Introduction and Design Rules*, MCNC MEMS Technology Applications Center, 3021 Cornwallis Road, Research Triangle Park, NC, Oct. 1994.